Journal of the Korean Physical Society, Vol. 73, No. 9, November 2018, pp. 1283∼1288

Light Coupling between Plasmonic Nanowire and Nanoparticle

Kyoung-Ho Kim
Department of Physics, Chungbuk National University, Cheongju 28644, Korea

You-Shin No*
Department of Physics, Konkuk University, Seoul 05029, Korea

(Received 30 August 2018, in final form 7 September 2018)

In this work, we investigate polarization-dependent excitation of the propagating surface plasmon polariton (SPP) modes in gold nanowires (Au NWs) combined with gold nanoparticles (Au NPs). The light coupling from focused light to SPPs on Au NWs is investigated for different structural combinations of Au NWs with Au NPs, using full-wave finite-element numerical simulations. The results show that the excitation of SPPs changes remarkably on varying the orientation of the NP on NW or the polarization angle of the incident light. Metallic NWs combined with NPs can be applied to the polarization-resolved SPP coupling in various optical and optoelectronic devices including photonic circuits and optical sensors.

PACS numbers: 42.55.Sa, 73.20.Mf, 42.82.Et, 78.67.Bf
Keywords: Surface plasmon polaritons, Gold nanowire, Gold nanoparticle, Finite-element method simulations
DOI: 10.3938/jkps.73.1283

I. INTRODUCTION

Low-dimensional materials such as nanowires (NWs) and nanoparticles (NPs) are excellent platforms for understanding the fundamentals of light-matter interaction in small-sized objects with sizes comparable to the wavelength of light and for developing high-performance optical and optoelectronic devices [1–8]. Metallic NWs and NPs, in particular, have attracted tremendous attention because of their unprecedented optical response in the visible-wavelength regime [5–14]. For example, NWs and NPs composed of noble metals can support collective oscillations of free carriers in a metallic object, called surface plasmon polaritons (SPPs). The SPPs in metallic NWs can propagate along the NW axis with wavelengths shorter than their wavelengths in free space, resulting in highly confined light concentration on the NWs, which facilitates ultracompact photonic circuits suitable for large-scale integration [5,6,12–14]. In metallic NPs, localized SPPs can be excited in a small volume, and it enables to develop highly sensitive optical sensors for molecules [7, 8]. The excitation of SPPs in such low-dimensional materials is significantly affected by the structural configurations of the NWs and NPs and the condition of the incident light [6,9–12,14]. Understanding the mechanism of the light coupling from external light to SPPs in NWs and NPs is essential for achieving high-performance subwavelength optical and optoelectronic devices. In this work, we study the excitation of SPPs resulting from the illumination of focused light onto the surface of Au NWs, for different structural configurations of Au NWs with Au NPs and for changes in the polarization of the incident light. We investigate the light coupling from focused light to the propagating SPPs, using the full-wave three-dimensional (3D) finite-element method (FEM) and quantitatively characterize the coupling strength using the power flux ratio between the incident light and propagating SPPs on a single Au NW. Our numerical calculations show that the light coupling is strongly dependent on the relative positions of the NPs on the NWs, with respect to the NW tip and the substrate. In addition, the results demonstrate that the coupling strength can be tuned by changing the polarization angle of the incident light. The tunable nature of the excitation of SPPs on metallic NWs combined with NPs can be used for polarization-resolved SPP coupling in various key photonic elements including waveguides, switches, and sensors.

II. RESULTS AND DISCUSSION

Figure 1(a) schematically illustrates our simulation configuration, which consists of a Au NW with circular cross-section of diameter D_{NW}, along the y-axis on a SiO_2 substrate. An incident Gaussian beam, linearly

*E-mail: ysno@konkuk.ac.kr; Fax: +82-2-3436-5382

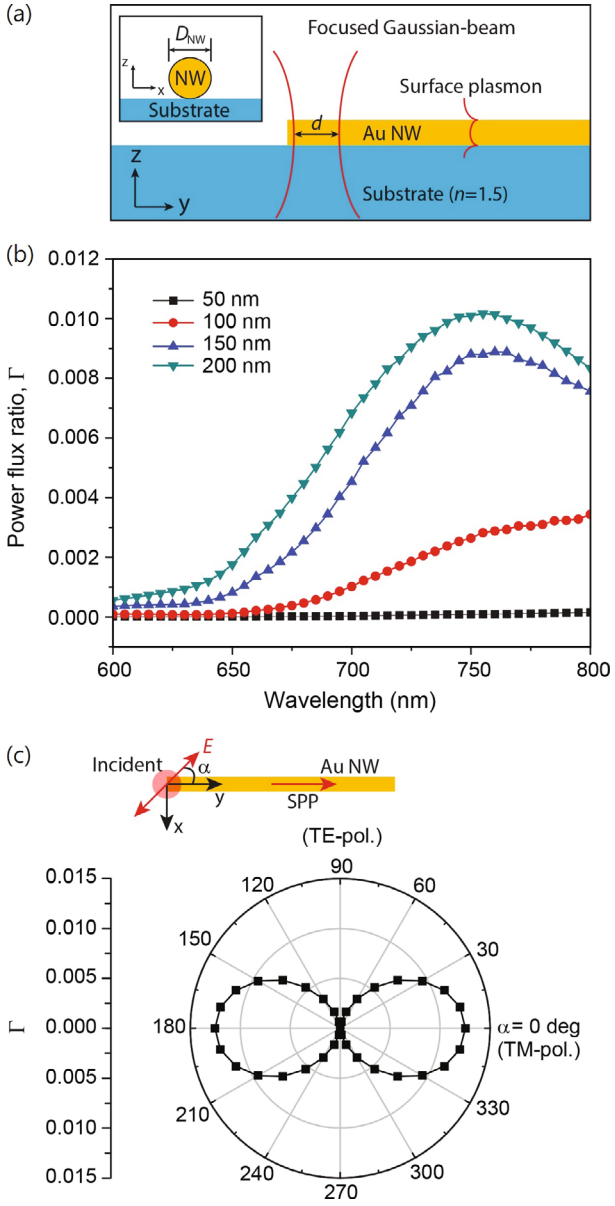

Fig. 1. (Color online) Excitation of a surface plasmon mode by focused Gaussian beam. (a) Schematic illustration of the excitation of a surface plasmon mode on a gold nanowire (Au NW), using a linearly polarized focused Gaussian beam. The Au NW with diameter D_{NW} was placed on top of an SiO_2 substrate with a refractive index of 1.5. The spot size of the focused Gaussian beam was d. (b) Calculated spectrum of the power flux ratio, Γ, for different D_{NW} of 50 (black, squares), 100 (red, circles), 150 (blue, triangles), and 200 nm (cyan, inversed triangles). The focused Gaussian beam with electric field parallel to the NW axis was illuminated onto the edge of the Au NW. d was 1 μm. (c) Calculated Γ as a function of the polarization angle of the incident light α. The focused Gaussian beam was illuminated on the edge of the Au NW with D_{NW} of 200 nm (inset). The excitation wavelength was 760 nm.

polarized in a direction parallel to the NW axis, is illuminated from the top and focused on one end of the NW, with a focused beam spot size of d defined by the beam waist diameter. SPPs are then excited on the surface of the Au NW where a metal-dielectric interface is formed. These SPPs are coupled to propagating plasmonic waveguide modes supported by the NW and propagate along the NW axis. We used 3D FEM (COMSOL 5.3a; wave optics module) to numerically characterize the light coupling in our plasmonic system. First, we obtained the incident power P_{inc} by calculating the z-component of the time-averaged Poynting vectors of the incident Gaussian beam passing through the center of an imaginary detection plane of area 3.0×3.0 μm^2 that sufficiently contained the Gaussian beam illumination area. In addition, we calculated the y-component of the time-averaged Poynting vectors at a point 10.0 μm distant from the NW end where the light coupling occurred, to obtain the propagating electromagnetic power P_{SPP} delivered by the plasmonic waveguide mode. A detection plane of area 3.0×3.0 μm^2, including both the cross section of the NW and the fields of the plasmonic waveguide modes, was used to calculate P_{SPP}. Next, we introduced the power flux ratio Γ, which is defined as the ratio of P_{SPP} to P_{inc}, to quantitatively characterize the combined effect of the incident light coupling and SPP propagation. For a single propagating plasmonic waveguide mode, we can simply writhe the relation of these quantities as

$$P_{SPP} = \eta_c e^{-L/L_{SPP}} P_{inc} = \Gamma P_{inc}. \quad (1)$$

Here, η_c is the coupling efficiency of the incident light to the propagating plasmonic waveguide mode at the end of the NW. L_{SPP} and L are the propagation length of the plasmonic waveguide mode and the distance of the detection position from the NW end, respectively. In Fig. 1(b), we simulate various Au NWs with different diameters of 50 (black, squares), 100 (red, circles), 150 (blue, triangles), and 200 nm (cyan, inversed triangles), and estimate their Γ values as a function of the incident wavelength ranging from 600 to 800 nm. For the NW with a D_{NW} of 50 nm, the propagating electromagnetic powers at the detection position was negligible for all wavelengths. However, the Γ values for the NWs with $D_{NW} \geq 100$ nm gradually increased with increasing wavelength, reached a maximum, and started decreasing. For example, the maximum Γ value of the NW with D_{NW} of 200 nm was estimated as ~ 0.010 at a wavelength of 760 nm. In addition, the larger-diameter NWs showed greater Γ values in the overall spectral range. The wavelength-dependent variation in the power flux ratio for a given NW can be primarily attributed to the different spectral response in coupling strength and the momentum mismatch between the vertically illuminated incident Gaussian beam and the propagating plasmonic waveguide modes. This can explain the negligible or very low Γ values of small NWs as well as the low Γ values for long wavelength in the given NW. Moreover, the

frequency-dependent dielectric function of Au has an effect on the depth of field penetration inside the metal and, consequently, is responsible for the short propagation length and high metallic loss at short wavelengths. We further investigated the light-coupling properties by systematically varying the angle of the incident polarization of the Gaussian beam, with respect to the NW axis (α in inset schematic, Fig. 1(c)). The Au NW with D_{NW} of 200 nm was used and the incident conditions were kept the same as those in Fig. 1(b). The polar plot of the Γ values in Fig. 1(c) clearly displays the polarization dependent light coupling from focused light to the propagating SPPs; the maximum (minimum) Γ value was achieved when the polarization of the incident beam was aligned parallel, *i.e.*, transverse-magnetic polarization, (normal, transverse-electric polarization) to the NW axis. Due to symmetry of the incident field and the NW geometry, the light scattering from the tip of the NW, which reduces momentum mismatch, was suppressed when the incident polarization deviated from the NW axis, which directly led to a rapid decrease in the coupling efficiency η_{c} and subsequently Γ.

Based on the understanding of light coupling in a single Au NW of Fig. 1, we introduced a single spherical Au NP to the surface of a single Au NW to control the light-coupling characteristics. Figure 2(a) displays the simulation geometry. In the schematic cross section, the 50 nm sized Au NP that lay on the surface of the NW made a polar angle φ with respect to the vertical axis in the NW cross-sectional coordinate. In addition, the NP was located at a position 1 μm away from the end of NW. The D_{NW} was set to 200 nm. The incident Gaussian beam was shifted and top-illuminated on the position of the NP to excite SPPs. Figure 2(b) shows the results of systematically increasing the angle φ from 0° to 120°. We repeated the same calculation process in Fig. 1(b) to estimate the Γ values for the TM- (black, squares) and TE-polarized incidences (red, circles) at the wavelength of 760 nm. Here, we used the distance from the NP to the detection position as L in Eq. (1) to estimate Γ. We observed several important features. First, the estimated Γ values for both polarizations were significantly lower than those in Fig. 1(b). It is known that, when an incident beam is projected on terminations of a single NW, the strong light-matter interactions near the terminations give rise to additional scattering wavevectors that effectively compensate the momentum mismatch between the incident beam and the propagating plasmonic waveguide modes. However, the incident beam in Fig. 2 was shifted 1 μm in the y-direction so that it primarily interacted with the NW body, which prevented the generation of scattering wavevectors, limiting the coupling efficiency η_{c} in the Γ value. Second, the estimated Γ values for the TM-polarized incident beam showed no noticeable response to the variations in the position of the NPs. The incident beam interacted mainly with the NW body and the tip of the NW, owing to its electric field oscillation direction. Third, the estimated Γ val-

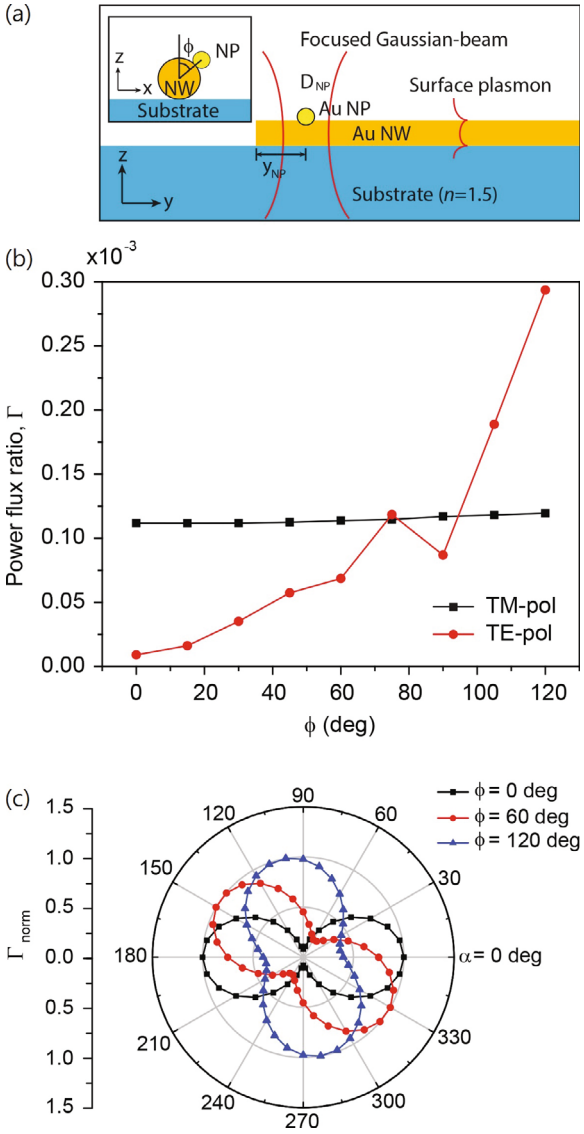

Fig. 2. (Color online) Excitation of a surface plasmon mode on the Au NW with a single gold nanoparticle (Au NP). (a) Schematic illustration of the Au NW with an Au NP. The Au NP with diameter D_{NP} was placed on the surface of the Au NW with its orientation tilted at an angle of φ with respect to the z-axis. The focused Gaussian beam was shifted from the edge of the NW to the Au NP by a distance of y_{NP}. (b) Calculated power flux ratio Γ, as a function of φ for TE- ($\alpha = 0°$, red, circles) and TM-polarized ($\alpha = 90°$, black, squares) incident Gaussian beams. D_{NW} and D_{NP} were 200 and 50 nm, respectively. y_{NP} was 1 μm. The spot size of the focused beam, d, was 1 μm and the excitation wavelength was 760 nm. (c) Calculated normalized power flux ratio Γ_{norm}, as a function of the polarization angle of the incident light, α for different φ of 0 (black), 60 (red), and 120° (blue). Γ_{norm} is the value of Γ normalized with respect to the maximum value of Γ for α. The relative scales are 1, 1.4 and 2.7 for φ of 0, 60, and 120°, respectively. The structural parameters were the same as those in (b). The spot size of the focused beam, d, was 1 μm and the excitation wavelength was 760 nm.

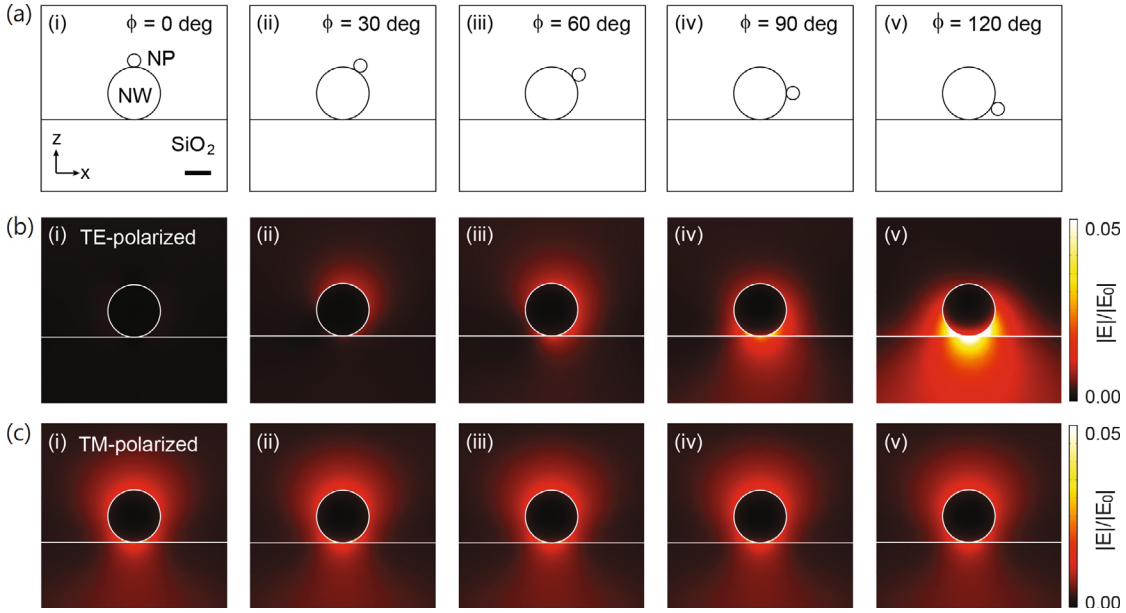

Fig. 3. (Color online) Mode profiles of propagating surface plasmon modes on the Au NW. (a) Cross-sectional configurations of NWs and NPs with different angles of $\varphi = 0°$ (i), $\varphi = 30°$ (ii), $\varphi = 60°$ (iii), $\varphi = 90°$ (iv), and $\varphi = 120°$ (v). (b, c) Electric field profiles of propagating plasmonic waveguide modes for different φ of 0, 30, 60, 90, and 120° when TE- (b) and TM-polarized (c) focused Gaussian beams illuminated the Au NW with Au NP. The structural parameters were the same as those in Fig. 2(b). The electric field profiles were obtained on the plane perpendicular to the NW axis, at a point 10 μm away from the edge of the NW. The electric fields were normalized with respect to the maximum electric field of the incident Gaussian beam at the focal point. The spot size of the focused beam, d, was 1 μm and the excitation wavelength was 760 nm. The scale bar was 100 nm.

ues for the TE-polarized incident beam exhibited a considerable increase as the angle increased. For example, when the NP was on top of the NW ($\varphi = 0°$), negligible power transmission (P_{SPP}) was detected. However, for $\varphi = 120°$, the Γ value increased 32-fold, compared to the value at $\varphi = 0°$. For high angles of φ, the NP on the NW body can actively interact with the incident fields oscillating in the direction normal to the NW axis and provide scattering wavevectors that enable light coupling to the propagating waveguide modes. This interaction can be maximized when the NP on the NW body is close to the substrate because the interfaces of the NW, NP, and substrate form a complex 3D geometry that is advantageous for rich light scattering and for the generation of scattering wavevectors. In Fig. 2(c), we further investigate the correlation between the incident polarization and the position of the NP on the NW body. For three different NP and NW geometries, with angles φ of 0° (black, squares), 60° (red, circles), and 120° (blue, triangles), we gradually increased the incident polarization from 0° to 360°, calculated the Γ values for each geometry, and normalized them with their respective maximum values. The polar plots of the normalized Γ values showed clear polarization-dependent light-coupling behaviors. Notably, the polarization axis that produced a maximum Γ value varied gradually as the angle defining the relative positions of the NP and NW increased.

We further confirmed our analysis by visualizing the propagating SPPs in Fig. 3. Figure 3(a) shows various cross-sectional configurations of NWs and NPs with different angles of $\varphi = 0°$ (i), $\varphi = 30°$ (ii), $\varphi = 60°$ (iii), $\varphi = 90°$ (iv), and $\varphi = 120°$ (v). For each configuration, we calculated the electric field intensity distributions at the detection position for both TE- and TM-polarized illuminations. Under TE-polarized illumination, the electric field intensity of the propagating plasmonic waveguide mode increased as the angle increased. In particular, when the NP was close to the substrate (*i.e.*, $\varphi = 120°$), a strong field intensity distribution was clearly observed between the NW and the substrate. As explained, the oscillation direction of the incident beam and the relative position of the NP caused rich light scattering at the interfaces of the NP, NW, and substrate, enabling efficient light coupling to the plasmonic waveguide modes. On the contrary, for TM-polarized illumination, weak and nearly constant electric field intensity distributions were observed for all angles. The results in Fig. 3 strongly support the results in Fig. 2 and confirm our previous analyses.

Finally, to investigate the interactions between the NP and the NW tip, we varied the longitudinal position of the NP on the NW (y_{NP}) and the polar angle φ. We repeated the calculation process in Fig. 2(b) and estimated the power flux ratios for both TE- (Γ_{TE}) and TM-polarized incidences (Γ_{TM}). For TE-polarized illumination, the relative longitudinal position of the NP, with

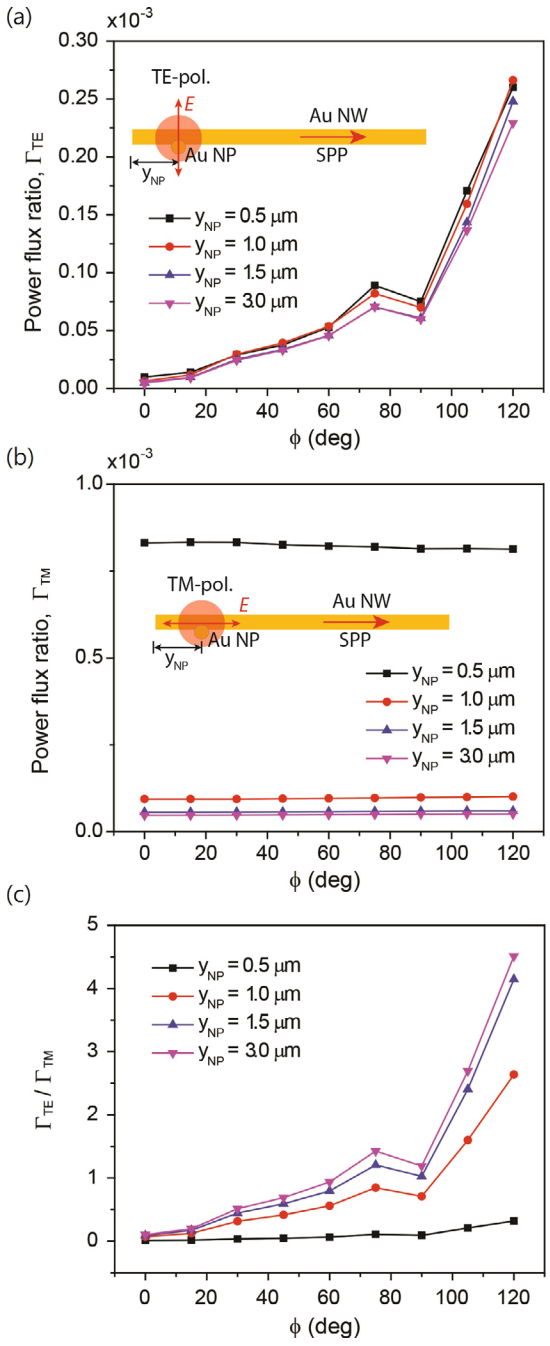

Fig. 4. (Color online) Tunable characteristics of polarization-dependent excitation of surface plasmon modes. (a) Power flux ratio, $\Gamma_{\rm TE}$, for a TE-polarized incident focused beam (inset) for different $y_{\rm NP}$ of 0.5 (black, squares), 1.0 (red, circles), 1.5 (blue, triangles), and 3.0 mm (purple, inversed triangles), as a function of the Au NP tilting angle φ. (b) Power flux ratio, $\Gamma_{\rm TM}$, for TM-polarized incident focused beam (inset) for different $y_{\rm NP}$ of 0.5 (black, squares), 1.0 (red, circles), 1.5 (blue, triangles), and 3.0 mm (purple, inversed triangles), as a function of φ. (c) Ratio of $\Gamma_{\rm TE}$ and $\Gamma_{\rm TM}$ for different $y_{\rm NP}$ of 0.5 (black, squares), 1.0 (red, circles), 1.5 (blue, triangles), and 3.0 mm (purple, inversed triangles), as a function of φ. $D_{\rm NW}$, $D_{\rm NP}$, d, and the excitation wavelength were set to 200, 50, 1000, and 760 nm, respectively, for (a) through (c).

respect to the tip of the NW, revealed small NW-tip-NP interaction effect on the light coupling. Figure 4(a) shows that the $\Gamma_{\rm TE}$ values, as a function of the angle φ, exhibit almost the same trend for various longitudinal positions of 0.5, 1.0, 1.5, and 3.0 μm. A slight decrease in the $\Gamma_{\rm TE}$ value was observed as the longitudinal distance was increased. It can be understood that since the light coupling with the oscillation direction normal to the NW axis is already insensitive to the position of the incident beam center on the NW body, the addition of 50 nm sized NPs does not make considerable changes. Figure 4(b) displays very low $\Gamma_{\rm TM}$ values when $y_{\rm NP}$ is greater than 1.0 μm and they showed a small variation in the values with increase in the distance and an φ-independent behavior. We note that, for the case of $y_{\rm NP} = 0.5$ μm, the estimated Γ values were relatively high for all φ, compared to the other cases (*i.e.*, $y_{\rm NP} = 1.0$, 1.5, 3.0 μm), because of the direct interactions between the incident beam with a spot size of 1 μm and the NW tip. In Fig. 4(c), we calculated the ratio of $\Gamma_{\rm TE}/\Gamma_{\rm TM}$ as a function of the φ. The plot revealed that, for small values of φ, the light coupling in TE- versus TM-polarized incidence was very low, regardless of the longitudinal distance of the NP from the NW tip. However, for high values of φ, the light coupling under the TE-polarization incidence dominated that of the TM-polarization and the ratio of $\Gamma_{\rm TE}/\Gamma_{\rm TM}$ depended on the distance of the NP from the NW tip; the maximum ratio of $\Gamma_{\rm TE}/\Gamma_{\rm TM}$ was ~ 4.5 at $y_{\rm NP} = 3.0$ μm and $\varphi = 120°$. Taken together, these results can be useful in designing light-coupling experiments of NW and NP, by providing a good reference for TE- versus TM-polarized illuminations.

III. CONCLUSION

In conclusion, we investigated the light-coupling characteristics of a single Au NW and the combined structure of a single Au NW and NP. A full 3D FEM simulation was conducted to numerically characterize the light coupling in various structures with different incident polarizations and NW-NP geometries. We first studied the light coupling in a single NW, quantitatively, by defining the power flux ratio, defined as $\Gamma = P_{\rm SPP}/P_{\rm inc}$, for various wavelengths and incident polarizations. Then, we proposed a more complicated structure consisting of a single NW and NP. We introduced geometrical parameters of φ and $y_{\rm NP}$, which represented the polar angle with respect to the vertical axis in the NW cross-sectional coordinate and the longitudinal distance between the NP and NW tip, respectively. From the simulations, we found that the light coupling became stronger when the NP on the NW was close to the high-index substrate, which was advantageous for rich light scattering to generate scattering wavevectors and for compensating the momentum mismatch in the coupling. In addition, we investigated the interaction effect between the NP and

the NW tip on the light coupling for TE- versus TM-polarized incidences. For small values of φ, the interaction effect was negligible for both polarizations. However, the interaction depending on the longitudinal distance of y_{NP} affected the ratio of $\Gamma_{\mathrm{TE}}/\Gamma_{\mathrm{TM}}$, providing a good guideline for light coupling using a linearly polarized incident beam. We believe that our simulation result can be useful for studies on the light coupling between various key photonic elements including metallic waveguides.

ACKNOWLEDGMENTS

This work was supported by the Basic Science Program of the National Research Foundation of Korea (NRF) funded by the Ministry of Education (2018R1C1B3001130).

REFERENCES

[1] B. Z. Tian, X. L. Zheng, T. J. Kempa, Y. Fang, N. F. Yu, G. H. Yu, J. L. Huang and C. M. Lieber, Nature **449**, 885 (2007).

[2] P. Avouris, M. Freitag and V. Perebeinos, Nat. Photonics **2**, 341 (2008).

[3] R. X. Yan, D. Gargas and P. D. Yang, Nat. Photonics **3**, 569 (2009).

[4] A. I. Kuznetsov, A. E. Miroshnichenko, M. L. Brongersma, Y. S. Kivshar and B. Luk'yanchuk, Science **354**, 846 (2016).

[5] Y. Fedutik, V. V. Temnov, O. Schops, U. Woggon and M. V. Artemyev, Phys. Rev. Lett. **99**, 136802 (2007).

[6] A. L. Pyayt, B. Wiley, Y. N. Xia, A. Chen and L. Dalton, Nat. Nanotechnol. **3**, 660 (2008).

[7] V. Giannini, A. I. Fernández-Domínguez, S. C. Heck and S. A. Maier, Chemical Reviews **111**, 3888 (2011).

[8] N. J. Halas, S. Lal, W-S. Chang, S. Link and P. Nordlander, Chemical Reviews **111**, 3913 (2011).

[9] Y. R. Fang, H. Wei, F. Hao, P. Nordlander and H. X. Xu, Nano Lett. **9**, 2049 (2009).

[10] J. A. Hutchison, S. P. Centeno, H. Odaka, H. Fukumura, J. Hofkens and H. Uji-i, Nano Lett. **9**, 995 (2009).

[11] T. Kang, W. Choi, I. Yoon, H. Lee, M. K. Seo, Q. H. Park and B. Kim, Nano Lett. **12**, 2331 (2012).

[12] X. Xiong, C. L. Zou, X. F. Ren, A. P. Liu, Y. X. Ye, F. W. Sun and G. C. Guo, Laser Photonics Rev. **7**, 901 (2013).

[13] Z. L. Zhang, Y. R. Fang, W. H. Wang, L. Chen and M. T. Sun, Adv. Sci. **3**, 1500215 (2016).

[14] H-S. Ee, Y-S. No, J. Kim, H-G. Park and M-K. Seo, Opt. Lett. **43**, 2889 (2018).